Journal of the Optical Society of America B
OPTICAL PHYSICS

Electromagnetically induced acoustic wave transparency in a diamond mechanical resonator

QIZHE HOU,[1,*] WANLI YANG,[2,5] CHANGYONG CHEN,[3] AND ZHANGQI YIN[4,6]

[1]National Laboratory of Solid State Microstructures and School of Physics, Nanjing University, Nanjing 210093, China
[2]State Key Laboratory of Magnetic Resonance and Atomic and Molecular Physics, Wuhan Institute of Physics and Mathematics, Chinese Academy of Sciences, Wuhan 430071, China
[3]Institute of Physics and Mechanical and Electrical Engineering, Shaoguan University, Shaoguan 512000, China
[4]Center for Quantum Information, Institute for Interdisciplinary Information Sciences, Tsinghua University, Beijing 100084, China
[5]e-mail: ywl@wipm.ac.cn
[6]e-mail: yinzhangqi@mail.tsinghua.edu.cn
*Corresponding author: houqizhe1988@126.com

Received 27 June 2016; revised 14 September 2016; accepted 14 September 2016; posted 14 September 2016 (Doc. ID 269247); published 10 October 2016

We propose a potentially practical scheme for realization of electromagnetically induced acoustic wave transparency (EIAT) in a high-Q single-crystal diamond mechanical resonator. Based on the dynamical strain-mediated coupling mechanism, we establish Λ-type and Δ-type transition structures in the subspace spanned by the ground states of the nitrogen-vacancy center, which drives the system into a coherent dark state, the system typically becoming transparent to the acoustic field, giving rise to the EIAT phenomenon. The physical picture behind EIAT is interpreted by using the framework of dressed states. Our work opens up possibilities to utilize this hybrid system as a building block to construct a spin-based physical material for quantum information processing and quantum optics applications, such as "slow sound" and enhanced nonlinear effects.

OCIS codes: (270.1670) Coherent optical effects; (270.5585) Quantum information and processing; (230.1040) Acousto-optical devices.

http://dx.doi.org/10.1364/JOSAB.33.002242

1. INTRODUCTION

As one of the well-known nonlinear optical effects, the electromagnetically induced transparency (EIT) effect [1–3] has received a great deal of attention in the past few years because it has disclosed new possibilities for nonlinear optics and quantum information processing (QIP), such as light storage [4,5], ultraslow light propagation [6–8], lasing without inversion [9], enhanced susceptibilities [10], and enhancement of nonlinear interactions [11] and dispersion effects [12,13]. Recently, a series of publications have investigated the analogues of the EIT effect by using acoustic waves and have demonstrated the phenomenon of acoustic transparency and slow-sound propagation under certain conditions [14–16]. To date, EIT and elated EIT-like effects have been theoretically investigated and experimentally observed in a variety of quantum systems, i.e., atomic systems [17–19], solid-state systems [20], superconductors [21], plasmonics [22], metamaterials [23], optomechanics [24–29], electronics [30], photonic crystals [31], and whispering-gallery-mode microresonators [32–36]. In the EIT process in a simple atomic medium, the three-level atoms (usually emerging as the Λ-, Ξ-, and V-type structures) are excited by two electromagnetic fields, where a strong control laser (coupling field) induces a narrow spectral transparency window for the weak probe laser beam (probe field). The physical mechanism of the EIT phenomenon can be explained equivalently from the dressed state basis referring to Fano interference [37], or the picture of bright and dark states [38].

Among solid-state systems, for instance, the diamond nitrogen-vacancy (NV) center has become one of the most promising solid-state platforms for QIP and quantum optics thanks to its long coherent properties [39–49] and optical addressability [50,51]. Previous works have focused on the EIT effect of the NV center from theoretical and experimental aspects [52–56]. However, the above-mentioned EIT effects take place only inside the all-optical region. In the microwave region with respect to the ground states of the NV center, there is a lack of an effective method for driving the system into a coherent dark state, the system typically becoming transparent to the probe field, giving rise to the EIT phenomenon. Here, by using the dynamical strain-mediated coupling mechanism in a high-Q single-crystal diamond mechanical resonator (DMR) [57–70], we establish suitable transition structures in the subspace spanned by the ground states of the NV center. The purpose of the present paper is to bring the original optical

phenomena into the realm of acoustic waves, namely, electromagnetically induced acoustic wave transparency (EIAT). The key point of our proposal is that the direct coupling between the lattice strain field and the NV center spins could be used to construct a Λ-type or Δ-type transition structure for the EIAT effect, and enable coherent spin–phonon interactions in the quantum regime, which could mark an important step toward engineering such a hybrid quantum device capable of investigating and simulating significant quantum optics and QIP. Our work is based on recent experimental and theoretical progress, e.g., a demonstration on the direct strain-coupling process with strain coupling strength of about 2 MHz inside the DMR via crystal vibration [59–61], and a very recent report about NV center-strain couplings exceeding 10 GHz for optical transitions [62]. Via quantum control of the NV center spin, the system shows a single standard acoustic transparency window in the general Λ-type transition case, and more complex quantum interference and coherent phenomena exist in the Δ-type transition case, such as three multiple transparency windows. We emphasize that switching between the single EIAT window and three multiple EIAT windows can be realized by adjusting the key system parameters. Additionally, the group velocity of the strain field is also discussed, and this hybrid system can be used as a building block to construct a "slow sound" solid-state physical material. The physical picture behind EIAT is interpreted by using the framework of dressed states.

2. SYSTEM AND MODEL

As illustrated in Fig. 1(a), the system under consideration is a monolithic hybrid quantum device DMR including a diamond cantilever with many embedded NV centers. A high-Q single-crystal DMR can be achieved in experiment with excellent nanofabrication techniques [57]. The NV centers in diamond are highly susceptible to deformations of the surrounding lattice; therefore, vibration due to the ground mechanical mode of the nanoresonator changes the local strain where the NV center is located, and gives rise to an effective, strain-induced electric field [71,72]. In general, the strain field can be produced by means of a thin piezoelectric [59–66] or piezomagnetic [73,74] film grown on the surface of the diamond layer, where the piezoelectric or piezomagnetic film behaves as a transducer

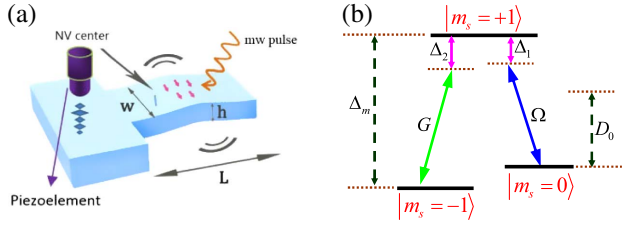

Fig. 1. (a) The system under consideration is a DMR containing many embedded NV centers, where the NV center spins are coupled to a cantilever that is resonantly driven by a piezoelement. (b) Energy levels of the ground-state of the NV center, where the transition $|+1\rangle\leftrightarrow|0\rangle$ is driven by a strong microwave field with Rabi frequency Ω, and the phonon strain field with Rabi frequency G has been employed to drive the transition $|+1\rangle\leftrightarrow|-1\rangle$. Here, $\Delta_{1(2)}$ are the detunings.

that transforms the signal between the external electric or magnetic field signal and the lattice vibration. When applying a voltage (magnetic field) across the piezoelectric film (piezomagnetic film), the strain field formed into a DMR. This implies that the strain induced by an oscillating cantilever modulates the energy of the ground-state spin levels, and the strain field can be well controlled by the external voltage or magnetic field.

Each NV center embedded in the DMR is negatively charged with two unpaired electrons located at the vacancy, usually treated as electron spin-1; thus, each NV center has a spin-triplet ground state. The nonaveraged electronic spin–spin interaction leads to energy splitting between $|^3A, m_s=0\rangle$ (labeled by $|0\rangle$) and $|^3A, m_s=\pm1\rangle$ (labeled by $|\pm1\rangle$) with the zero-field splitting about $D_0/2\pi\simeq 2.87$ GHz [75]. Meanwhile, the degeneracy of the levels $|^3A, m_s=\pm1\rangle$ can be lifted by employing an external magnetic field B_0 (i.e., $B_0>102$ mT), which could shift the level $|-1\rangle$ to be below the level $|0\rangle$ [76]. The external magnetic field with z-axis component B_z induces level splitting between $|\pm1\rangle$ with the width $\Delta_m=g_s\mu_B B_z/\hbar$, where $g_s\simeq 2$, μ_B represents the Bohr magneton, and we assume that the z axis is aligned with the NV center symmetry axis.

We first study individual NV center spin embedded in the DMR. Here the coherent strain driving of the NV center is based on the sensitive response of the NV center to strain in the diamond host lattice. In the present system, the uniaxial strain field from lattice vibration leads to direct coupling of the two electronic spin states $|+1\rangle$ and $|-1\rangle$, which is a dipole-forbidden transition ($m_s=2$), i.e., the microwave field is inaccessible to drive this transition $|+1\rangle\leftrightarrow|-1\rangle$ [71]. We model the strain field by an effective electric field E_i $(i=x,y,z)$, where the strain-induced displacements change the electron density of the crystal, resulting in the local electric field. Therefore, the corresponding strain-coupling Hamiltonian for the NV center takes the form (in units of $\hbar=1$, hereafter) [42,67]

$$H_{\rm NV}=(D_0+\epsilon_\parallel E_z)S_z^2+g_s\mu_B B_z S_z - \epsilon_\perp[E_x(S_xS_y+S_yS_x)+E_y(S_x^2-S_y^2)], \quad (1)$$

where S_i $(i=x,y,z)$ are the spin-1 operators. $\epsilon_{\parallel(\perp)}$ represents the strain coupling constant along the direction parallel (perpendicular) to the NV center symmetry axis.

3. EIAT PHENOMENON

In this section, we will investigate the phenomenon of EIAT in this hybrid system, under the Λ-type transition case and the Δ-type transition case. Based on the strain-coupling mechanism, suitable transition structures in the ground-state subspace for realization of the EIAT effect could be established, where the microwave field and the strain field can be well controlled by the Rabi frequency of the microwave pulse and the external voltage or magnetic field, respectively.

A. Λ-type EIAT

As stated previously, the spin-triplet ground states (including $|+1\rangle$, $|0\rangle$, and $|-1\rangle$) of the NV center are of interest to us. Here, each NV center is subject to the local electric field that results from the strain field, with frequency ω_p and intensity ϵ_p, whose perpendicular component leads to the transition

$|+1\rangle \leftrightarrow |-1\rangle$. Another microwave spin manipulation with frequency ω_c and intensity ε_c is applied to the NV centers, which drives the transition $|+1\rangle \leftrightarrow |0\rangle$, as illustrated in Fig. 1(b). In the interaction picture, the Hamiltonian of the whole system is written as

$$H = \Delta_2\sigma_{+1,+1} + \Delta\sigma_{0,0} - (G\sigma_{+1,-1} + \Omega\sigma_{+1,0} + \text{H.c.})/2, \quad (2)$$

where $\sigma_{ij} = |i\rangle\langle j|$ $(i,j = 0, \pm 1)$ are the NV center projection operators. $\Omega = \mu_{0,+1}\varepsilon_c/2\hbar$ and $G = \mu_{-1,+1}\varepsilon_p/2\hbar$ represent the Rabi frequencies of the microwave field and strain field, respectively, where μ_{ij} $(i,j = 0, \pm 1)$ represent the dipole matrix elements of the transition $|i\rangle \leftrightarrow |j\rangle$. Here $\Delta_{1(2)} = \omega_{+1} - \omega_{0(-1)} - \omega_{c(p)}$ and $\Delta = \Delta_2 - \Delta_1$ represent the detunings, and ω_i $(i = 0, \pm 1)$ are the frequencies of level $|i\rangle$. Hereafter, we set the level $|-1\rangle$ as the energy zero point.

The equations of motion for the density matrix elements are given by

$$\dot{\rho}_{+1,-1} = -(\gamma_1 + i\Delta_2)\rho_{+1,-1} + \frac{i\Omega\rho_{0,-1}}{2} + \frac{iG(\rho_{-1,-1} - \rho_{+1,+1})}{2}, \quad (3)$$

$$\dot{\rho}_{+1,0} = -(\gamma_2 + i\Delta_1)\rho_{+1,0} + \frac{iG\rho^*_{0,-1}}{2} + \frac{i\Omega(\rho_{0,0} - \rho_{+1,+1})}{2}, \quad (4)$$

$$\dot{\rho}_{0,-1} = -(\gamma_3 + i\Delta)\rho_{0,-1} - \frac{iG\rho^*_{+1,0}}{2} + \frac{i\Omega^*\rho_{+1,-1}}{2}, \quad (5)$$

where $\rho_{ij} = \langle i|\rho|j\rangle$ $(i,j = 0, \pm 1)$, $\gamma_{1(2)}$ are the decay rates from $|+1\rangle$ to $|-1\rangle$ $(|0\rangle)$, and γ_3 is the decay rate from $|0\rangle$ to $|-1\rangle$; $*$ denotes the complex conjugate.

Assuming that all NV centers occupy the ground state $|-1\rangle$ initially, we have $\rho_{-1-1} = 1$, $\rho_{+1,+1} = \rho_{0,0} = 0$. Setting $\dot{\rho}_{+1,-1} = \dot{\rho}_{+1,0} = \dot{\rho}_{0,-1} = 0$, the steady-state solution of off-diagonal density matrix element $\rho_{+1,-1}$ has the following form:

$$\rho_{+1,-1} = 2iG(\gamma_3 + i\Delta)/[4(\gamma_1 + i\Delta_2)(\gamma_3 + i\Delta) + |\Omega|^2]. \quad (6)$$

According to the well-known relations $P = \varepsilon_0\chi E$ and $P = N\mu_{ij}\rho_{ij}$ [77], where ε_0 is the permittivity of a vacuum, χ is the complex electric susceptibility, E is the strength of the electromagnetic field, N is the number density of the medium, and P is the intensity of polarization of the medium, we can obtain the linear susceptibility $\chi = N\mu_{ij}\rho_{ij}/\varepsilon_0 E = N\mu_{-1,+1}\rho_{+1,-1}/\varepsilon_0\varepsilon_p$ with the real part $\text{Re}(\chi) = K[\Delta_2(\Delta^2 + \gamma_3^2) - \Delta|\Omega|^2/4]/2Z$ and imaginary part $\text{Im}(\chi) = K[\gamma_1(\gamma_3^2 + \Delta^2) + \gamma_3|\Omega|^2/4]/2Z$, with $K = N|\mu_{-1,+1}|^2/2\varepsilon_0$, and $Z = (\gamma_1\gamma_3 - \Delta_2\Delta + |\Omega|^2/4)^2 + (\gamma_3\Delta_2 + \gamma_1\Delta)^2$. For simplicity, our calculation is in units of K. In the present model, the real part of the susceptibility $\text{Re}(\chi)$ is proportional to the dispersion coefficient of the medium, and its imaginary part $\text{Im}(\chi)$ reflects the absorption response of the media on the probe field.

In Fig. 2(a), we plot the imaginary part of the susceptibilities $\text{Im}(\chi)$ as a function of probe detuning Δ_2 under different Rabi frequencies Ω, where the parameters Ω and Δ_2 can be tuned by applying an adjustable external magnetic field. From Fig. 2(a), one can find that the strain field is absorbed completely by the DMR if the microwave coupling field is turned off $(\Omega = 0)$ in the resonant case $\Delta_2 = 0$. Once the microwave coupling field is applied, i.e., $\Omega = 1.5$, the medium is transparent to the strain field because $\text{Im}(\chi)$ equals zero in the resonant case. This means that the strong microwave coupling field $(G \ll \Omega)$ changes the absorption response of the DMR to the strain field, and leads to the occurrence of a single standard EIAT window. We call this phenomenon EIAT. Because of quantum interference introduced by the driving field, the acoustic wave can propagate without absorption under the appropriate conditions. This is similar to the result of EIT at optical frequencies, but the typical transition frequencies in DMR are much lower.

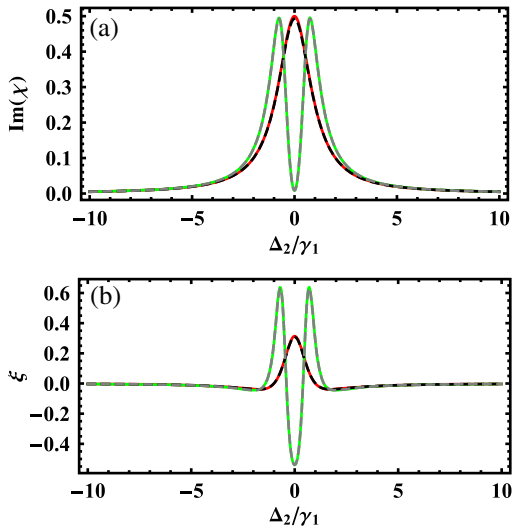

Fig. 2. (a) Imaginary part of the susceptibility $\text{Im}(\chi)$ and (b) the quantity ξ as functions of detuning Δ_2. The red solid and green solid lines represent the approximate analytical results of the different driving cases with $\Omega = 0$ and $\Omega = 1.5$, respectively. The corresponding numerical simulations without any approximations are represented by the black dashed and gray dashed lines, respectively. The other parameters are set as $G = 0.01$, $\gamma_1 = 1$, $\gamma_3 = 0.01$, and $\Delta = \Delta_2$.

An interesting characteristic of optical EIT is the slow-down of light propagation resulting from a strong dispersion effect [6–8]. Based on this driving interference effect, we will mimic the phenomenon of "slowing light" as "slowing sound" in the present system. The group velocity of the probe field is given by $v_g = v/n_g$, with sound propagating speed $v \simeq 17.5$ km/s in pure diamond [78] and group index $n_g = n_r + 2\pi\omega_p\partial\,\text{Re}(\chi)/\partial\omega_p$ [79], where $n_r = 1 + 2\pi\,\text{Re}(\chi)$ is the refractive index of the DMR. This means that group velocity v_g can reduced, and even be zero, if positive dispersion is realized, i.e., $\partial\,\text{Re}(\chi)/\partial\omega_p > 0$ [6]. In addition, the group velocity v_g can be increased, and even be negative, for the negative dispersion case with $\partial\,\text{Re}(\chi)/\partial\omega_p < 0$ [80,81]. In order to describe the phenomenon of "slowing sound" more quantitatively, here we define a quantity $\xi = 2\pi\,\text{Re}(\chi) + 2\pi\omega_p\partial\,\text{Re}(\chi)/\partial\omega_p = n_g - 1$, where $\xi < 0$ means supraliminal acoustic propagation, and subliminal acoustic propagation requires that the condition $\xi > 0$ can be well met.

In Fig. 2(b), the quantity ξ is plotted as a function of probe detuning Δ_2 under different microwave driving cases, where the quantity ξ is always larger than zero and reaches its maximum in the resonant case $(\Delta_2 = 0)$ if the microwave coupling field is absent; this means that subliminal acoustic propagation occurs. In the presence of the microwave driving field, the quantity ξ changes from a single wave crest into the doublet

of a wave crest with larger magnitude during the process of a frequency sweep. This indicates that the propagation of the acoustic strain field changes from subliminal to supraliminal, then again to subliminal. This demonstrates that the speed of the acoustic propagation can be easily tuned with probe detuning. The reason for the appearance of the doublet of a wave crest is the presence of a doublet of dressed states produced by the cancelation of opposite contributions from two different resonances. To get a clear picture of the dependence of the absorption response of the DMR on the parameter space $\{\Delta_1, \Delta_2\}$, we plot the values of $\mathrm{Im}(\chi)$ in Fig. 3. An interesting feature is that the absorption feature vanishes when detuning Δ_1 equals Δ_2; this is consistent with the generation condition of optical EIT with two-photon resonance. Once the detuning Δ_1 is very large, the absorption spectrum is essentially that of a two-level system with an additional narrow Raman peak close to the $\Delta = 0$ case.

B. Δ-type EIAT

The difference from the Λ-type transition case is that an additional microwave field is applied to drive the transition path $|-1\rangle \leftrightarrow |0\rangle$, as shown in Fig. 4. In the Δ-type transition case, a pair of microwave driving fields with Rabi frequencies $\Omega_{1(2)}$ create the transition $|+1\rangle \leftrightarrow |0\rangle$ ($|0\rangle \leftrightarrow |-1\rangle$), and the transition $|+1\rangle \leftrightarrow |-1\rangle$ is driven by the strain field with Rabi frequency λ, where $\lambda \ll \Omega_{1(2)}$.

The interaction Hamiltonian of the whole system is

$$H_1 = \delta_2\sigma_{-1,-1} + (\delta_1+\delta_2)\sigma_{+1,+1} - (\Omega_1\sigma_{+1,0} + \Omega_2\sigma_{0,-1} + \lambda e^{-i\delta t}\sigma_{+1,-1} + \mathrm{H.c.})/2, \quad (7)$$

where $\delta_1 = \omega_{+1} - \omega_0 - \omega_{c1}$, $\delta_2 = \omega_0 - \omega_{c2}$, $\delta_3 = \omega_{+1} - \omega_q$, and $\delta = \delta_1 + \delta_2 - \delta_3$. $\omega_{c1(2)}$ and ω_q are the frequencies of the microwave fields and strain field, respectively.

Taking the dissipative and dephasing effects into account, the density matrix equations can be written as [3]

$$\dot{\rho} = -i[H_1, \rho] + \mathcal{L}\rho, \quad (8)$$

with

$$\begin{aligned}\mathcal{L}\rho = {} & \Gamma_{31}(2\sigma_{-1,+1}\rho\sigma_{+1,-1} - \sigma_{+1,+1}\rho - \rho\sigma_{+1,+1})/2 \\ & + \Gamma_{32}(2\sigma_{0,+1}\rho\sigma_{+1,0} - \sigma_{+1,+1}\rho - \rho\sigma_{+1,+1})/2 \\ & + \Gamma_{21}(2\sigma_{-1,0}\rho\sigma_{0,-1} - \sigma_{0,0}\rho - \rho\sigma_{0,0})/2 \\ & + \gamma_{2d}(2\sigma_{0,0}\rho\sigma_{0,0} - \sigma_{0,0}\rho - \rho\sigma_{0,0})/2 \\ & + \gamma_{3d}(2\sigma_{+1,+1}\rho\sigma_{+1,+1} - \sigma_{+1,+1}\rho - \rho\sigma_{+1,+1})/2, \end{aligned} \quad (9)$$

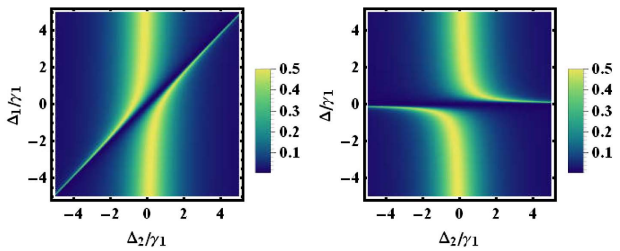

Fig. 3. Imaginary part of the susceptibility $\mathrm{Im}(\chi)$: left, as a function of detunings Δ_2 and Δ_1; and right, as a function of detunings Δ_2 and Δ. The other parameters are set as $\Omega = 1.5$, $G = 0.01$, $\gamma_1 = 1$, and $\gamma_3 = 0.01$.

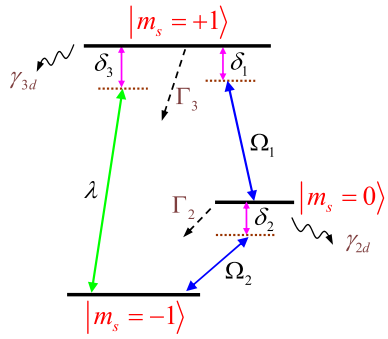

Fig. 4. Levels of Δ-type transition of the NV center system, where the transition $|+1\rangle \leftrightarrow |0\rangle$ ($|0\rangle \leftrightarrow |-1\rangle$) is coupling with strong microwave fields with Rabi frequencies $\Omega_{1(2)}$. The phonon strain field with Rabi frequency λ has been employed to drive the transition $|+1\rangle \leftrightarrow |-1\rangle$.

where the first, second, and third terms in the right-hand side describe the spontaneous emission from state $|+1\rangle$ to states $|-1\rangle$ ($|0\rangle$), and from state $|0\rangle$ to state $|-1\rangle$, with dissipative rates Γ_{31} (Γ_{32}) and Γ_{21}, respectively. The fourth and fifth terms describe the dephasing of the states $|0\rangle$ and $|+1\rangle$ with dephasing rates γ_{2d} and γ_{3d}, respectively. For convenience, we define the total spontaneous emission rates and the coherent decay rates of the state $|0\rangle$ ($|+1\rangle$) as $\Gamma_2 = \Gamma_{21}$ ($\Gamma_3 = \Gamma_{31} + \Gamma_{32}$) and $\gamma_2' = \Gamma_2 + \gamma_{2d}$ ($\gamma_3' = \Gamma_3 + \gamma_{3d}$), respectively, where $\Gamma_{31} \simeq \Gamma_{32} = \Gamma_3/2$ has been assumed.

The motion equations for all of the elements of the density matrix are listed as follows:

$$\begin{aligned}
\dot{\rho}_{-1,-1} &= \Gamma_2\rho_{0,0} + \Gamma_3\rho_{+1,+1}/2 - i[\lambda e^{-i\delta t}\rho_{-1,+1} - \lambda e^{i\delta t}\rho_{+1,-1} + \Omega_2(\rho_{-1,0} - \rho_{0,-1})]/2, \\
\dot{\rho}_{-1,0} &= -\gamma_2'\rho_{-1,0}/2 - i[-\lambda e^{i\delta t}\rho_{+1,0} - 2\delta_2\rho_{-1,0} + \Omega_1\rho_{-1,+1} + \Omega_2(\rho_{-1,-1} - \rho_{0,0})]/2, \\
\dot{\rho}_{-1,+1} &= -\gamma_3'\rho_{-1,+1}/2 - i[\lambda e^{i\delta t}(\rho_{-1,-1} - \rho_{+1,+1}) - 2(\delta_1+\delta_2)\rho_{-1,+1} + \Omega_1\rho_{-1,0} - \Omega_2\rho_{0,+1}]/2, \\
\dot{\rho}_{0,-1} &= -\gamma_2'\rho_{0,-1}/2 - i[\lambda e^{-i\delta t}\rho_{0,+1} + 2\delta_2\rho_{0,-1} - \Omega_1\rho_{+1,-1} - \Omega_2(\rho_{-1,-1} - \rho_{0,0})]/2, \\
\dot{\rho}_{0,0} &= -\Gamma_2\rho_{0,0} + \Gamma_3\rho_{+1,+1}/2 - i[\Omega_1(\rho_{0,+1} - \rho_{+1,0}) + \Omega_2(\rho_{0,-1} - \rho_{-1,0})]/2, \\
\dot{\rho}_{0,+1} &= -(\gamma_2' + \gamma_3')\rho_{0,+1}/2 - i[\lambda e^{i\delta t}\rho_{0,-1} - 2\delta_1\rho_{0,+1} + \Omega_1(\rho_{0,0} - \rho_{+1,+1}) - \Omega_2\rho_{-1,+1}]/2, \\
\dot{\rho}_{+1,-1} &= -\gamma_3'\rho_{+1,-1}/2 + i[\lambda e^{-i\delta t}(\rho_{-1,-1} - \rho_{+1,+1}) - 2(\delta_1+\delta_2)\rho_{+1,-1} + \Omega_1\rho_{0,-1} - \Omega_2\rho_{+1,0}]/2, \\
\dot{\rho}_{+1,0} &= -(\gamma_2' + \gamma_3')\rho_{+1,0}/2 + i[Ge^{-i\delta t}\rho_{-1,0} - 2\delta_1\rho_{+1,0} + \Omega_1(\rho_{0,0} - \rho_{+1,+1}) - \Omega_2\rho_{+1,-1}]/2, \\
\dot{\rho}_{+1,+1} &= -\Gamma_3\rho_{+1,+1} + i[\lambda e^{-i\delta t}\rho_{-1,+1} - \lambda e^{i\delta t}\rho_{+1,-1} - \Omega_1(\rho_{+1,0} - \rho_{0,+1})]/2.
\end{aligned} \quad (10)$$

Based on the population conservation rule $\rho_{-1,-1} + \rho_{0,0} + \rho_{+1,+1} = 1$, after eliminating the term $\rho_{-1,-1}$, we can write Eq. (10) in a compact form:

$$\dot{R} = MR - A,$$

where

$$R = (\rho_{0,0}, \rho_{+1,+1}, \rho_{+1,-1}, \rho_{-1,0}, \rho_{0,+1}, \rho_{+1,0}, \rho_{-1,+1}, \rho_{0,-1})^T \quad (11)$$

and the constant vector is

$$A = (0, 0, -i\lambda \exp(-i\delta t)/2, i\Omega_2/2, 0, 0, i\lambda \exp(i\delta t)/2, -i\Omega_2/2)^T, \quad (12)$$

with T the matrix transpose. The form of matrix M can be deduced from the coefficients of Eq. (10).

Both the vector A and matrix M can be divided into terms with different time dependence [82,83]:

$$A = A_0 + \lambda \exp(-i\delta t)A_1 + \lambda \exp(i\delta t)A_{-1}, \quad (13)$$

and

$$M = M_0 + \lambda \exp(-i\delta t)M_1 + \lambda \exp(i\delta t)M_{-1}, \quad (14)$$

with A_0, $A_{\pm 1}$, M_0, $M_{\pm 1}$ the constant matrices. Thus, we obtain

$$\dot{R} + A_0 + \lambda \exp(-i\delta t)A_1 + \lambda \exp(i\delta t)A_{-1} = (M_0 + \lambda \exp(-i\delta t)M_1 + \lambda \exp(i\delta t)M_{-1})R. \quad (15)$$

By using the Floquet theorem [84], we can obtain the stationary solution with respect to R. In the case of $\lambda \ll \Omega_{1(2)}$, the Floquet harmonic expansion of R could be truncated at the first order; then we can obtain R that contains only terms at the harmonics of the detuning δ as

$$R = R_0 + \lambda \exp(-i\delta t)R_1 + \lambda \exp(i\delta t)R_{-1}. \quad (16)$$

Substituting Eq. (16) into Eq. (15) and equating the coefficients of the different harmonics of δ and the corresponding powers of λ, the solutions for R_0 and R_1 are given by

$$R_0 = M_0^{-1}A_0, R_1 = (M_0 + i\delta)^{-1}(A_1 - M_1R_0). \quad (17)$$

On the other hand, the linear susceptibility χ of the weak probe field in the present system is proportion to $[R_1]_3$, where $[R_1]_3$ is determined from the third elements of R_1 [38], and the index of refraction (absorption) is obtained by the real (imaginary) part of χ.

In Fig. 5, we plot the value of Im(χ) and the quantity ξ as functions of the probe detuning δ_3. One can find that the DMR shows an electromagnetic response that closely resembles the EIT in an optical system, and the strain field is absorbed completely by the medium when $\Omega_1 = \Omega_2 = 0$ in the resonant case with $\delta_3 = 0$, as illustrated in Fig. 5(a). If we drive only the transition $|+1\rangle \leftrightarrow |0\rangle$, similar to the Λ-type case in the above section, a transparency window on the strain field exists, as shown in Fig. 5(b). Once a pair of microwave driving fields are turned on simultaneously, as illustrated in Fig. 5(c), three multiple transparent windows occur, among which the big transparent window occurs in the resonant case $\delta_3 = 0$, but the degree of the absorption response of the medium is weaker than the non-driving case ($\Omega_2 = 0$). In addition, the other two transparent windows appear symmetrically on both sides of the central window. This is because the added electromagnetic field in the Δ-type transition case can change the maximum transmission of the probe field, the sensitivity of

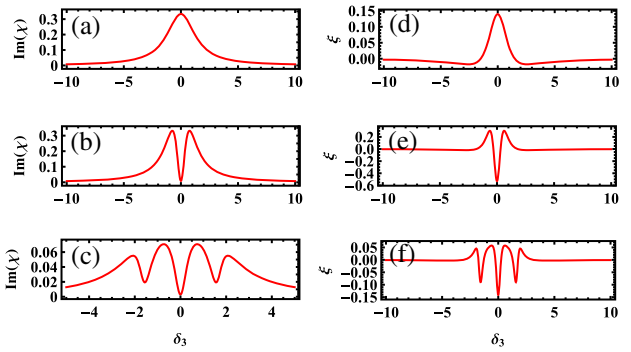

Fig. 5. Imaginary part of the susceptibility Im(χ) (left panel) and the quantity ξ (right panel) as functions of detuning δ_3 in different driving cases: (a, d) ($\Omega_1 = 0$, $\Omega_2 = 0$), (b, e) ($\Omega_1 = 1.5$, $\Omega_2 = 0$), and (c, f) ($\Omega_1 = 1.5$, $\Omega_2 = 1.5$). The other parameters are set as $\lambda = 0.01$, $\Gamma_{32} = \Gamma_{31} = 1$, $\Gamma_{21} = 0.01$, $\gamma_{2d} = 0.01$, $\gamma_{3d} = 1$, and $\delta_1 = \delta_2 = 0$.

the EIT on the loss of coherence, the splitting features of the EIT window, and the dependence of the probe transmission spectra on the total phase of the applied fields. As a result, three valleys on the quantity ξ appear, comparing with the single valley in the Λ-type case, as shown in Fig. 5(f). This implies that more complex quantum interference and coherent phenomena exist in the Δ-type case, and one can control the group velocity of the acoustic field in a more flexible way.

To obtain more physical characteristics about the dependence of response of the DMR system on the added microwave driving field, we first investigate the effect of the Rabi frequency Ω_2 on the probe absorption spectrum by setting the detuning $\delta_2 = 0$, as illustrated in Fig. 6, where we set the Rabi frequency of the microwave field Ω_1. When the Rabi frequency Ω_2 increases, the distance between the lateral EIAT windows and the central EIAT window widens, but the position of the central EIAT window is fixed, as shown in Fig. 6(a). More specifically, in Fig. 6(b), we plot the frequency interval between the central EIAT window and the lateral EIAT windows as a function of the Rabi frequency Ω_2; a linear relationship exists and the frequency interval equals the Rabi frequency Ω_2. Also, the influence from detuning δ_2 on the added microwave driving field is investigated in Fig. 7, which tells us that the position

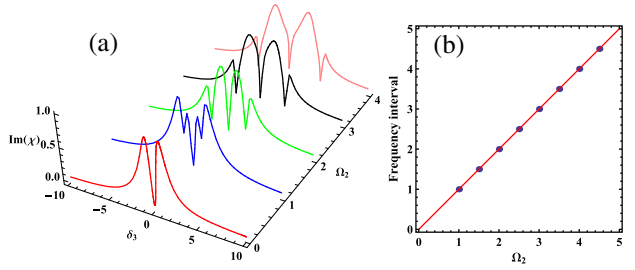

Fig. 6. (a) Value of Im(χ) as a function of detuning δ_3 and Rabi frequency Ω_2. (b) Frequency interval between the central EIAT window and the lateral EIAT window as a function of Rabi frequency Ω_2. The other parameters are set as $\lambda = 0.01$, $\Gamma_{32} = \Gamma_{31} = 1$, $\Gamma_{21} = 0.01$, $\gamma_{2d} = 0.01$, $\gamma_{3d} = 1$, $\Omega_2 = 1.5$, and $\delta_1 = \delta_2 = 0$.

of the central EIAT window varies obviously with the change of detuning δ_2, as illustrated in Fig. 7(a). In the same manner, we plot the frequency shift ($\delta_2 \neq 0$) with respect to the central EIAT window, compared with the resonant case ($\delta_2 = 0$), as a function of detuning δ_2 in Fig. 7(b). A similar linear relationship is found, and the frequency shift is equal to detuning δ_2 of the microwave driving field when specific parameters are set. In Fig. 7(c), the frequency interval between the central EIAT window and the lateral EIAT windows as a function of detuning δ_2 is also plotted. This verifies that the frequency interval equals the general Rabi frequency $\sqrt{\Omega_2^2 + \delta_2^2}$ of the added microwave driving field. Thus, both the Rabi frequency and detuning of the added microwave driving field Ω_2 could be effectively used to achieve frequency tuning of the EIAT windows. We emphasize that the switching between the single EIAT window and three multiple EIAT windows can be obtained by properly adjusting the system parameters.

In the following, we give the physical interpretation of the above novel phenomena in Figs. 6 and 7 by using the framework of dressed states [85,86]. In the present system, both energy levels $|-1\rangle$ and $|0\rangle$ will be spilled into a pair of dressed state levels under the strong driving of the external microwave driving field Ω_2, as illustrated in Fig. 8(b) [Fig. 8(a) is the simplified version of Fig. 4]; this effect is the well-known dynamical Stark splitting. The splitting width Ω_p equals the general Rabi frequency $\sqrt{\Omega_2^2 + \delta_2^2}$ of the driving field. In the case of the equal detuning of the microwave coupling field Ω_1 and probe field with $\delta_1 = \delta_3$, four transition paths $p_{1(2,3,4)}$ exist in the system, and every transition path could be treated as a Λ-type three-level system. In the four transition paths $p_{1(2,3,4)}$, the frequencies of the strain fields are equal in transition paths p_2 and p_3, and the frequencies of the strain fields in paths p_1 and p_4 have a positive and negative shift, respectively, compared with paths p_2 and p_3. Therefore, the central EIAT window is attributed to transition paths p_2 and p_3, and the lateral EIAT window is attributed to transition paths p_1 and p_4. In addition, the frequency shift in transition paths p_1 and p_4 depends on the splitting width Ω_p in the dressed state framework, which is consistent with the analyses about Figs. 6(b) and 7(c). Furthermore, compared with the resonant case ($\delta_2 = 0$), when detuning $\delta_2 \neq 0$, the frequency shift corresponding to the central EIAT window equals detuning δ_2 of the microwave driving field, agreeing with the description of Fig. 7(b).

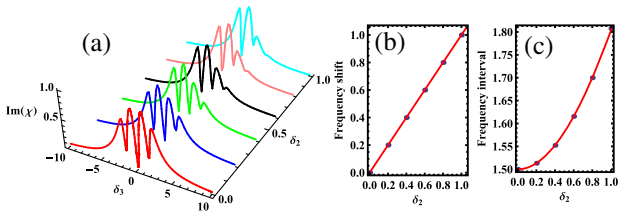

Fig. 7. (a) Value of Im(χ) as a function of detuning δ_3 and Rabi frequency Ω_2. (b) Frequency shift of the central EIAT window as a function of detuning δ_2 in the detuning case with $\delta_2 \neq 0$. (c) Frequency interval between the central EIAT window and the lateral EIAT window as a function of detuning δ_2. The other parameters are set as $\lambda = 0.01$, $\Gamma_{32} = \Gamma_{31} = 1$, $\Gamma_{21} = 0.01$, $\gamma_{2d} = 0.01$, $\gamma_{3d} = 1$, $\Omega_1 = \Omega_2 = 1.5$, and $\delta_1 = 0$.

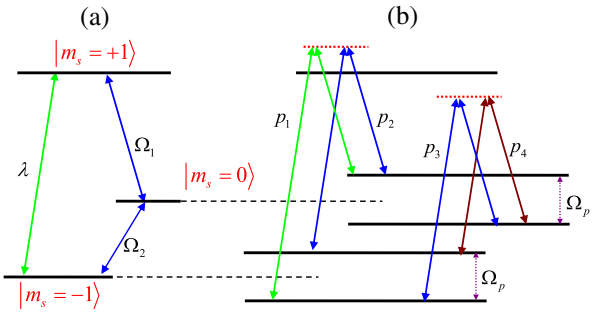

Fig. 8. (a) Bare-state and (b) dressed-state energy levels of the Fig. 4. Here, $p_{1(2,3,4)}$ represent four transition paths in the case of $\delta_1 = \delta_3$, and Ω_p is the splitting width on energy levels $|m_s = -1\rangle$ and $|m_s = 0\rangle$ under the driving of microwave field Ω_2.

4. DISCUSSION AND CONCLUSION

We briefly address the experimental feasibility of our scheme. One of inherent advantages of this strain-coupled spin-resonator system is that no additional components are required to tune the coupling strength due to the intrinsic nature of the coupling. In addition, this NV center-resonator system requires no functionalization of the resonator, compared with other hybrid mechanical systems [59]. In our model, by properly adjusting the external magnetic field, we can make energy level $|-1\rangle$ close to level $|0\rangle$. In this case, the decay rate in the transition $|-1\rangle \leftrightarrow |0\rangle$ is weak compared with the transition $|+1\rangle \leftrightarrow |-1\rangle$ ($|0\rangle$). Additionally, the strength and detuning of the microwave fields can be easily adjusted. The strain field can also be well controlled by the external voltage or magnetic field, and the magnitude of the strain is highly controlled, and is set by the cantilever's mode shape and amplitude of motion, the depth and lateral location of the NV center in the DMR, and the orientation of the NV center. On the other hand, the phenomenon of acoustic-wave-induced microwave transparency could also be realized in the present system by using a similar idea, i.e., using the acoustic strain field as the strong coupling field, and using the microwave field as the weak probe field, which will induce a narrow spectral transparency window for the microwave field.

Additionally, our result could be expanded into the quantum regime. For instance, the coupling strength and the frequency of the DMR can be calculated from Euler–Bernoulli thin beam elasticity theory if we take a doubly clamped diamond beam with $L \gg w, h$ [87]. As the strain is linear to its position within small displacement, we can express the electric field E_y in Eq. (1) into the quantized term $E_y = E_0(a + a^\dagger)$, with $a^\dagger$ (a) the creation (destruction) operator of the mode of the DMR, and E_0 the perpendicular strain resulting from the zero point motion of the beam. Under the rotating wave approximation, the interaction Hamiltonian has the form $H_i = g_0(\sigma_i^+ a + a^\dagger \sigma_i^-)$, where $\sigma_i^\pm$ is the Pauli operator for the ith NV center. For an NV center near the surface of the beam, we have the individual coupling strength $g_0/2\pi \simeq 180\sqrt{\hbar/(L^3 w\sqrt{\rho E})}$ [67] with ρ and E the mass density and Young's modulus of diamond, respectively. We can estimate the vibrational frequency $\omega_m/2\pi \sim 2$ GHz and the individual coupling $g_0/2\pi \sim 4$ kHz for a beam of dimensions

$(L, w, h) = (0.5, 0.05, 0.05)$ μm. Additionally, a long spin relaxation time of $T_1 \sim 100$ s [88] and spin dephasing time $T_2 = 10$ ms [41] at low temperature are achieved in experiment. These parameters are suitable for the realization of EIAT in the present system.

In conclusion, we propose a potential scheme to observe EIAT in a DMR system. We demonstrate that a single and three multiple EIAT windows occur in the Λ-type and Δ-type transition cases, respectively, and switching between the single and three EIAT windows can be obtained by properly adjusting the system parameters. Additionally, the group velocity of the acoustic strain field was also discussed. With the NV center's long quantum coherence time and diamond's low mechanical losses, this hybrid system provides a unique environment to engineer spin–phonon interaction, and can be used as a building block to construct a "slow sound" solid-state physical material. We think our investigation could promote related phonon-based QIP applications, such as phonon-based information storage and propagation.

Funding. National Natural Science Foundation of China (NSFC) (11474153, 11574353, 11274351, 61435007, 11474177); PCSIRT (IRT1243).

Acknowledgment. We thank Shi-Liang Zhu for enlightening discussions. W. L. Yang was supported by the NSFC (Grants 11574353 and 11274351). Z. Q. Yin was supported by the NSFC (Grants 61435007 and 11474177).

REFERENCES

1. K. J. Boller, A. Imamoğlu, and S. E. Harris, "Observation of electromagnetically induced transparency," Phys. Rev. Lett. **66**, 2593–2596 (1991).
2. S. E. Harris, "Electromagnetically induced transparency," Phys. Today **50**(7), 36–42 (1997).
3. M. Fleischhauer, A. Imamoglu, and J. P. Marangos, "Electromagnetically induced transparency: optics in coherent media," Rev. Mod. Phys. **77**, 633–673 (2005).
4. D. F. Phillips, A. Fleischhauer, A. Mair, R. L. Walsworth, and M. D. Lukin, "Storage of light in atomic vapor," Phys. Rev. Lett. **86**, 783–786 (2001).
5. C. Liu, Z. Dutton, C. H. Behroozi, and L. V. Hau, "Observation of coherent optical information storage in an atomic medium using halted light pulses," Nature **409**, 490–493 (2001).
6. L. V. Hau, S. E. Harris, Z. Dutton, and C. H. Behroozi, "Light speed reduction to 17 metres per second in an ultracold atomic gas," Nature **397**, 594–598 (1999).
7. M. Xiao, Y.-Q. Li, S.-Z. Jin, and J. Gea-Banacloche, "Measurement of dispersive properties of electromagnetically induced transparency in rubidium atoms," Phys. Rev. Lett. **74**, 666–669 (1995).
8. M. S. Bigelow, N. N. Lepeshkin, and R. W. Boyd, "Observation of ultraslow light propagation in a ruby crystal at room temperature," Phys. Rev. Lett. **90**, 113903 (2003).
9. A. S. Zibrov, M. D. Lukin, D. E. Nikonov, L. Hollberg, M. O. Scully, V. L. Velichansky, and H. G. Robinson, "Experimental demonstration of laser oscillation without population inversion via quantum interference in Rb," Phys. Rev. Lett. **75**, 1499–1502 (1995).
10. A. S. Zibrov, M. D. Lukin, L. Hollberg, D. E. Nikonov, M. O. Scully, H. G. Robinson, and V. L. Velichansky, "Experimental demonstration of enhanced index of refraction via quantum coherence in Rb," Phys. Rev. Lett. **76**, 3935–3938 (1996).
11. S. E. Harris and L. V. Hau, "Nonlinear optics at low light levels," Phys. Rev. Lett. **82**, 4611–4614 (1999).
12. Y. Wu and X. Yang, "Electromagnetically induced transparency in *V*-, Λ-, and cascade-type schemes beyond steady-state analysis," Phys. Rev. A **71**, 053806 (2005).
13. Y. Wu, J. Saldana, and Y. Zhu, "Large enhancement of four-wave mixing by suppression of photon absorption from electromagnetically induced transparency," Phys. Rev. A **67**, 013811 (2003).
14. X.-T. Xie, W. Li, J. Li, W.-X. Yang, A. Yuan, and X. Yang, "Transverse acoustic wave in molecular magnets via electromagnetically induced transparency," Phys. Rev. B **75**, 184423 (2007).
15. A. Santillán and S. I. Bozhevolnyi, "Acoustic transparency and slow sound using detuned acoustic resonators," Phys. Rev. B **84**, 064304 (2011).
16. A. Santillán and S. I. Bozhevolnyi, "Demonstration of slow sound propagation and acoustic transparency with a series of detuned resonators," Phys. Rev. B **89**, 184301 (2014).
17. M. Mücke, E. Figueroa, J. Bochmann, C. Hahn, K. Murr, S. Ritter, C. J. Villas-Boas, and G. Rempe, "Electromagnetically induced transparency with single atoms in a cavity," Nature **465**, 755–758 (2010).
18. H. Yan, K.-Y. Liao, J.-F. Li, Y.-X. Du, Z.-M. Zhang, and S.-L. Zhu, "Bichromatic electromagnetically induced transparency in hot atomic vapors," Phys. Rev. A **87**, 055401 (2013).
19. A. Feizpour, M. Hallaji, G. Dmochowski, and A. M. Steinberg, "Observation of the nonlinear phase shift due to single post-selected photons," Nat. Phys. **11**, 905–909 (2015).
20. J. J. Longdell, E. Fraval, M. J. Sellars, and N. B. Manson, "Stopped light with storage times greater than one second using electromagnetically induced transparency in a solid," Phys. Rev. Lett. **95**, 063601 (2005).
21. S. Novikov, T. Sweeney, J. E. Robinson, S. P. Premaratne, B. Suri, F. C. Wellstood, and B. S. Palmer, "Raman coherence in a circuit quantum electrodynamics lambda system," Nat. Phys. **12**, 75–79 (2015).
22. S. Zhang, D. A. Genov, Y. Wang, M. Liu, and X. Zhang, "Plasmon-induced transparency in metamaterials," Phys. Rev. Lett. **101**, 047401 (2008).
23. N. Papasimakis, V. A. Fedotov, N. I. Zheludev, and S. L. Prosvirnin, "Metamaterial analog of electromagnetically induced transparency," Phys. Rev. Lett. **101**, 253903 (2008).
24. S. Weis, R. Rivière, S. Deléglise, E. Gavartin, O. Arcizet, A. Schliesser, and T. J. Kippenberg, "Optomechanically induced transparency," Science **330**, 1520–1523 (2010).
25. A. H. Safavi-Naeini, T. P. M. Alegre, J. Chan, M. Eichenfield, M. Winger, Q. Lin, J. T. Hill, D. E. Chang, and O. Painter, "Electromagnetically induced transparency and slow light with optomechanics," Nature **472**, 69–73 (2011).
26. H. Xiong, L.-G. Si, A.-S. Zheng, X. Yang, and Y. Wu, "Higher-order sidebands in optomechanically induced transparency," Phys. Rev. A **86**, 013815 (2012).
27. Y. Chang, T. Shi, Y.-x. Liu, C. P. Sun, and F. Nori, "Multistability of electromagnetically induced transparency in atom-assisted optomechanical cavities," Phys. Rev. A **83**, 063826 (2011).
28. S. Huang and G. S. Agarwal, "Electromagnetically induced transparency with quantized fields in optocavity mechanics," Phys. Rev. A **83**, 043826 (2011).
29. W. Z. Jia, L. F. Wei, Y. Li, and Y.-x. Liu, "Phase-dependent optical response properties in an optomechanical system by coherently driving the mechanical resonator," Phys. Rev. A **91**, 043843 (2015).
30. C. L. G. Alzar, M. A. G. Martinez, and P. Nussenzveig, "Classical analog of electromagnetically induced transparency," Am. J. Phys. **70**, 37–41 (2002).
31. X. Yang, M.-B. Yu, D.-L. Kwong, and C. W. Wong, "All-optical analog to electromagnetically induced transparency in multiple coupled photonic crystal cavities," Phys. Rev. Lett. **102**, 173902 (2009).
32. Q. Xu, S. Sandhu, M. L. Povinelli, J. Shakya, S.-H. Fan, and M. Lipson, "Experimental realization of an on-chip all-optical analogue to electromagnetically induced transparency," Phys. Rev. Lett. **96**, 123901 (2006).
33. K. Totsuka, N. Kobayashi, and M. Tomita, "Slow light in coupled-resonator-induced transparency," Phys. Rev. Lett. **98**, 213904 (2007).
34. B. Peng, Ş. K. Özdemir, W. Chen, F. Nori, and L. Yang, "What is and what is not electromagnetically induced transparency in whispering-gallery microcavities," Nat. Commun. **5**, 5082 (2014).

35. J. Kim, M. C. Kuzyk, K. Han, H. Wang, and G. Bahl, "Non-reciprocal Brillouin scattering induced transparency," Nat. Phys. **11**, 275–280 (2015).
36. C.-H. Dong, Z. Shen, C.-L. Zou, Y.-L. Zhang, W. Fu, and G.-C. Guo, "Brillouin-scattering-induced transparency and non-reciprocal light storage," Nat. Commun. **6**, 6193 (2015).
37. U. Fano, "Effects of configuration interaction on intensities and phase shifts," Phys. Rev. **124**, 1866–1878 (1961).
38. M. O. Scully and M. S. Zubairy, *Quantum Optics* (Cambridge University, 1997).
39. L. Childress, M. V. G. Dutt, J. M. Taylor, A. S. Zibrov, F. Jelezko, J. Wrachtrup, P. R. Hemmer, and M. D. Lukin, "Coherent dynamics of coupled electron and nuclear spin qubits in diamond," Science **314**, 281–285 (2006).
40. H. Bernien, B. Hensen, W. Praff, G. Koolstra, M. S. Blok, L. Robledo, T. H. Taminiau, M. Markham, D. J. Twitchen, L. Childress, and R. Hanson, "Heralded entanglement between solid-state qubits separated by three metres," Nature **497**, 86–90 (2013).
41. G. Balasubramanian, P. Neumann, D. Twitchen, M. Markham, R. Kolesov, N. Mizuochi, J. Isoya, J. Achard, J. Beck, J. Tissler, V. Jacques, P. R. Hemmer, F. Jelezko, and J. Wrachtrup, "Ultralong spin coherence time in isotopically engineered diamond," Nat. Mater. **8**, 383–387 (2009).
42. F. Dolde, H. Fedder, M. W. Doherty, T. Nöbauer, F. Rempp, G. Balasubramanian, T. Wolf, F. Reinhard, L. C. L. Hollenberg, F. Jelezko, and J. Wrachtrup, "Electric-field sensing using single diamond spins," Nat. Phys. **7**, 459–463 (2011).
43. C. G. Yale, B. B. Buckley, D. J. Christle, G. Burkard, F. J. Heremans, L. C. Bassett, and D. D. Awschalom, "All-optical control of a solid-state spin using coherent dark states," Proc. Natl. Acad. Sci. USA **110**, 7595–7600 (2013).
44. P. Rabl, P. Cappellaro, M. V. G. Dutt, L. Jiang, J. R. Maze, and M. D. Lukin, "Strong magnetic coupling between an electronic spin qubit and a mechanical resonator," Phys. Rev. B **79**, 041302 (2009).
45. P. Rabl, S. J. Kolkowitz, F. H. L. Koppens, J. G. E. Harris, P. Zoller, and M. D. Lukin, "A quantum spin transducer based on nanoelectromechanical resonator arrays," Nat. Phys. **6**, 602–608 (2010).
46. J.-B. You, W. L. Yang, Z.-Y. Xu, A. H. Chan, and C. H. Oh, "Phase transition of light in circuit-QED lattices coupled to nitrogen-vacancy centers in diamond," Phys. Rev. B **90**, 195112 (2014).
47. W. L. Yang, J. H. An, C. J. Zhang, C. Y. Chen, and C. H. Oh, "Dynamics of quantum correlation between separated nitrogen-vacancy centers embedded in plasmonic waveguide," Sci. Rep. **5**, 15513 (2015).
48. Z. Q. Yin, T. Li, X. Zhang, and L. M. Duan, "Large quantum superpositions of a levitated nanodiamond through spin-optomechanical coupling," Phys. Rev. A **88**, 033614 (2013).
49. Z.-T. Liang, X. Yue, Q. Lv, Y.-X. Du, W. Huang, H. Yan, and S.-L. Zhu, "Proposal for implementing universal superadiabatic geometric quantum gates in nitrogen-vacancy centers," Phys. Rev. A **93**, 040305(R) (2016).
50. F. Jelezko, T. Gaebel, I. Popa, A. Gruber, and J. Wrachtrup, "Observation of coherent oscillations in a single electron spin," Phys. Rev. Lett. **92**, 076401 (2004).
51. G. D. Fuchs, V. V. Dobrovitski, D. M. Toyli, F. J. Heremans, and D. D. Awschalom, "Gigahertz dynamics of a strongly driven single quantum spin," Science **326**, 1520–1522 (2009).
52. C. Wei and N. B. Manson, "Observation of the dynamic Stark effect on electromagnetically induced transparency," Phys. Rev. A **60**, 2540–2546 (1999).
53. E. A. Wilson, N. B. Manson, C. Wei, and L. Yang, "Perturbing an electromagnetically induced transparency in a Λ system using a low-frequency driving field. I. Three-level system," Phys. Rev. A **72**, 063813 (2005).
54. J.-H. Wu, G. C. L. Rocca, and M. Artoni, "Controlled light-pulse propagation in driven color centers in diamond," Phys. Rev. B **77**, 113106 (2008).
55. P. R. Hemmer, A. V. Turukhin, M. S. Shahriar, and J. A. Musser, "Raman-excited spin coherences in nitrogen-vacancy color centers in diamond," Opt. Lett. **26**, 361–363 (2001).
56. V. M. Acosta, K. Jensen, C. Santori, D. Budker, and R. G. Beausoleil, "Electromagnetically induced transparency in a diamond spin ensemble enables all-optical electromagnetic field sensing," Phys. Rev. Lett. **110**, 213605 (2013).
57. Y. Tao, J. M. Boss, B. A. Moores, and C. L. Degen, "Single-crystal diamond nanomechanical resonators with quality factors exceeding one million," Nat. Commun. **5**, 3638 (2014).
58. B. Khanaliloo, M. Mitchell, A. C. Hryciw, and P. E. Barclay, "High-*Q*/*V* monolithic diamond microdisks fabricated with quasi-isotropic etching," Nano Lett. **15**, 5131–5136 (2015).
59. P. Ovartchaiyapong, K. W. Lee, B. A. Myers, and A. C. B. Jayich, "Dynamic strain-mediated coupling of a single diamond spin to a mechanical resonator," Nat. Commun. **5**, 4429 (2014).
60. J. Teissier, A. Barfuss, P. Appel, E. Neu, and P. Maletinsky, "Strain coupling of a nitrogen-vacancy center spin to a diamond mechanical oscillator," Phys. Rev. Lett. **113**, 020503 (2014).
61. A. Barfuss, J. Teissier, E. Neu, A. Nunnenkamp, and P. Maletinsky, "Strong mechanical driving of a single electron spin," Nat. Phys. **11**, 820–824 (2015).
62. K. W. Lee, D. Lee, P. Ovartchaiyapong, J. Minguzzi, J. R. Maze, and A. C. B. Jayich, "Strain coupling of a mechanical resonator to a single quantum emitter in diamond," arXiv:1603.07680 (2016).
63. S. Meesala, Y.-I. Sohn, H. A. Atikian, S. Kim, M. J. Burek, J. T. Choy, and M. Lončar, "Enhanced strain coupling of nitrogen-vacancy spins to nanoscale diamond cantilevers," Phys. Rev. Appl. **5**, 034010 (2016).
64. E. R. MacQuarrie, T. A. Gosavi, N. R. Jungwirth, S. A. Bhave, and G. D. Fuchs, "Mechanical spin control of nitrogen-vacancy centers in diamond," Phys. Rev. Lett. **111**, 227602 (2013).
65. E. R. MacQuarrie, T. A. Gosavi, A. M. Moehle, N. R. Jungwirth, S. A. Bhave, and G. D. Fuchs, "Coherent control of a nitrogen-vacancy center spin ensemble with a diamond mechanical resonator," Optica **2**, 233–238 (2015).
66. E. R. MacQuarrie, T. A. Gosavi, S. A. Bhave, and G. D. Fuchs, "Continuous dynamical decoupling of a single diamond nitrogen-vacancy center spin with a mechanical resonator," Phys. Rev. B **92**, 224419 (2015).
67. S. D. Bennett, N. Y. Yao, J. Otterbach, P. Zoller, P. Rabl, and M. D. Lukin, "Phonon-induced spin-spin interactions in diamond nanostructures: application to spin squeezing," Phys. Rev. Lett. **110**, 156402 (2013).
68. K. V. Kepesidis, S. D. Bennett, S. Portolan, M. D. Lukin, and P. Rabl, "Phonon cooling and lasing with nitrogen-vacancy centers in diamond," Phys. Rev. B **88**, 064105 (2013).
69. Q. Xu, W. L. Yang, and Z.-Q. Yin, "Phonon induced two-mode squeezing of nitrogen-vacancy center ensembles," arXiv:1512.08605 (2015).
70. Z. Q. Yin, N. Zhao, and T. C. Li, "Hybrid opto-mechanical systems with nitrogen-vacancy centers," Sci. China Phys. Mech. Astron. **58**, 1–12 (2015).
71. J. R. Maze, "Properties of nitrogen-vacancy centers in diamond: the group theoretic approach," New J. Phys. **13**, 025025 (2011).
72. M. W. Doherty, F. Dolde, H. Fedder, F. Jelezko, J. Wrachtrup, N. B. Manson, and L. C. L. Hollenberg, "Theory of the ground-state spin of the NV^- center in diamond," Phys. Rev. B **85**, 205203 (2012).
73. J. Cai, F. Jelezko, and M. B. Plenio, "Hybrid sensors based on colour centres in diamond and piezoactive layers," Nat. Commun. **5**, 4065 (2014).
74. M. J. A. Kessler, E. M. Schuetz, G. Giedke, L. M. K. Vandersypen, M. D. Lukin, and J. I. Cirac, "Universal quantum transducers based on surface acoustic waves," Phys. Rev. X **5**, 031031 (2015).
75. N. B. Manson, J. P. Harrison, and M. J. Sellars, "Nitrogen-vacancy center in diamond: model of the electronic structure and associated dynamics," Phys. Rev. B **74**, 104303 (2006).
76. L. Jin, M. Pfender, N. Aslam, P. Neumann, S. Yang, J. Wrachtrup, and R.-B. Liu, "Proposal for a room-temperature diamond maser," Nat. Commun. **6**, 8251 (2015).
77. A. Yariv, *Quantum Electronics* (Wiley, 1989).
78. P. W. May, "Diamond thin films: a 21st-century material," Philos. Trans. R. Soc. A **358**, 473–495 (2000).
79. Z. Ficek and S. Swain, *Quantum Interference and Coherence: Theory and Experiments* (Springer, 2005).

80. A. M. Steinberg and R. Y. Chiao, "Dispersionless, highly superluminal propagation in a medium with a gain doublet," Phys. Rev. A **49**, 2071–2075 (1994).
81. L. J. Wang, A. Kuzmich, and A. Dogariu, "Gain-assisted superluminal light propagation," Nature **406**, 277–279 (2000).
82. X.-M. Hu and J. Xu, "Enhanced index and negative dispersion without absorption in driven cascade media," Phys. Rev. A **69**, 043812 (2004).
83. L.-G. Wang, S. Qamar, S.-Y. Zhu, and M. S. Zubairy, "Manipulation of the Raman process via incoherent pump, tunable intensity, and phase control," Phys. Rev. A **77**, 033833 (2008).
84. G. Floquet, "Sur les équations différentielles linéaires à coefficients périodiques," Ann. Sci. Ec. Normale Super. **12**, 47–88 (1883).
85. C. Cohen-Tannoudji and S. Reynaud, "Dressed-atom description of resonance fluorescence and absorption spectra of a multi-level atom in an intense laser beam," J. Phys. B **10**, 345–363 (1977).
86. C. Cohen-Tannoudji, J. Dupont-Roc, and G. Grynberg, *Atom-Photon Interactions* (Wiley-VCH, 1992).
87. L. Landau and E. Lifshitz, *Theory of Elasticity* (Butterworth-Heinemann, 1986).
88. A. Jarmola, V. M. Acosta, K. Jensen, S. Chemerisov, and D. Budker, "Temperature- and magnetic-field-dependent longitudinal spin relaxation in nitrogen-vacancy ensembles in diamond," Phys. Rev. Lett. **108**, 197601 (2012).